Evolution of the streamwise vortices in a coaxial jet controlled with micro flap actuators

K. ANGELE[*], N. KURIMOTO, Y. SUZUKI and N. KASAGI

The University of Tokyo, Tokyo 113-8656, Japan

A coaxial jet was actively controlled by a MEMS-fabricated micro flap actuator nozzle. The effect of different control modes on secondary azimuthal instabilities and the evolution of streamwise vortices were investigated by applying stereoscopic PIV to the cross-stream plane of the jet. Forcing with non-symmetric modes, in particular the least-stable helical mode, accelerates the evolution of the streamwise vortices through the enhancement of azimuthal instabilities. Although forcing is applied to the outer shear layer of the outer jet, the control effect is most pronounced in the inner shear layer of the inner jet. Unlike in the natural jet, streamwise vortices appear in the inner shear layer of the controlled jet. For forcing with the fundamental axisymmetric mode, a Strouhal number of the order of unity maximise the azimuthal instabilities and hence the counts of the streamwise vortices. The present result is in accordance with our previous experimental findings in the longitudinal plane, where the evolution of the primary vortices and mixing between the inner and the outer jets were examined through 2D-PIV and PLIF (Kurimoto et al., 2004, Active control of coaxial jet mixing with arrayed micro actuators. *Transactions of the Japanese Society of Mechanical Engineers*, pp. 31–38.) This emphasises the connection between primary and streamwise vortices and their significance in the mixing enhancement process. It is also found that the azimuthal wavelength under the present control scheme is almost the same as that of the natural jet and independent of the streamwise position.

Keywords: Coaxial jet; Control; Azimuthal instabilities; Streamwise vortices; PIV

1.   Introduction

Coaxial jets are commonly utilized in contexts where mixing between two streams is desired. In small-scale combustors such as micro gas turbines, mixing enhancement between fuel and air is generally required due to the inherently low Reynolds number. The ultimate goal of the present research is to generate a control system with which the vortical flow structures, and thereby the mixing between the inner and the outer jets, can be flexibly manipulated under various partial load conditions of small-scale combustors.

The development of two-dimensional and three-dimensional vortical structures and its connection to mixing has been extensively investigated in the plane mixing layer. In the mixing layer, two-dimensional primary vortices emerge due to the Kelvin–Helmholz (KH) instability. Small differences in the upstream conditions are amplified by the strain in the braid region between the KH vortices, and three-dimensional instabilities subsequently lead to the evolution of streamwise vortices before the breakdown to turbulence [11]. Breidenthal [4] employed a chemical reaction technique to quantify the mixing in the plane mixing layer. He concluded that mixing transition is a consequence of the onset of small-scale three-dimensional structures.

---

*Corresponding author. E-mail: kristian.angele@vattenfall.com

A sinuous disturbance in the spanwise direction, with a wavelength similar to that of the primary KH vortices, was observed. The amplitude of the disturbance grows in the downstream direction, but the length scales remain unchanged. The primary KH vortices remained two dimensional despite the presence of the sinuous disturbance. Pierrehumbert and Widnall [22] examined the stability of the plane mixing layer as an eigenvalue problem and found the spanwise instability, which was named the *translative instability*. Its spanwise wavelength was found to be two-thirds that of the primary KH vortices. Bernal and Roshko [3] conducted flow visualizations in the plane mixing layer. They show that the spanwise wavelength of the streamwise vortices is independent of the absolute velocity, the velocity ratio, the density ratio and the velocity profile of the initial shear layer. The ratio of the spanwise to the streamwise wavelengths was found to vary between 0.45 and 1.1, with a mean value of 0.67, in agreement with the predictions by Pierrehumbert and Widnall [22]. They concluded that the streamwise vortices play an important role in the process of mixing. Lasheras et al. [16] also conducted flow visualizations in the plane mixing layer. They proposed a scenario for the generation of streamwise vortices; spanwise vorticity in the braid region is tilted and stretched into pairs of streamwise vortices. They observed that the count of streamwise vortices increased in the downstream direction, which was explained by self-induction, stretching and tilting. It was also found that streamwise vortices could develop before the primary KH vortices, depending on the upstream conditions. The spanwise wavelength was found to be slightly smaller than that of the primary KH vortices.

It has been confirmed that the evolution of the streamwise vortices from the primary vortices, through the secondary instabilities, appears not only in the plane mixing layer, but also in jets. Martin and Meiburg [18, 19] observed counter-rotating streamwise vortices in their simulation of inviscid vortex filaments when axial disturbances were applied. Liepmann and Gharib [17] showed fingers in the azimuthal direction in their flow visualization of a single jet. They also found that the mode number is increased with the Reynolds number. The fingers developed into pairs of counter-rotating streamwise vortices and their relative importance, with respect to the primary vortex rings, increased in the downstream direction. Villermaux and Rehab [27] made mixing measurements of a coaxial jet of which the setup was developed by Rehab et al. [25]. Streamwise vortices are clearly observed in the shear layers.

Many studies of jet control have utilized acoustic forcing of the bulk flow (e.g., [7, 10]), or passive devices such as tabs (e.g. [24]) in order to manipulate the vortical structures and enhance the mixing. Helical forcing of a single jet for stabilisation of a lifted flame using piezo-electrical flaps was reported by Chao et al. [5]. Several azimuthal fingers were observed, but only one finger developed into a streamwise vortex in the observed region. Demare and Baillot [10] investigated the flame-stabilisation mechanism in an acoustically forced non-premixed axisymmetric single jet. They concluded that secondary instabilities and streamwise vortices are key ingredients in the mixing process and flame-stabilisation mechanism.

Our group has made a series of jet control studies with flap actuators mounted in the jet nozzle [24]. Kurimoto et al. [14] showed that a flapping Strouhal number (St) of unity maximises the density of strong primary vortex rings and hence the mixing between the inner and the outer jets. Kurimoto et al. [13] showed that for forcing with an *alternate mode* (for details, see subsection 2.3), the near-field mixing between the inner and the outer jets was significantly enhanced compared to the axisymmetric mode at $St = 1.0$. They attributed this fact to the enlargement of the primary vortices. Mitsuishi et al. [21] performed a direct numerical simulation (DNS) in a confined coaxial jet focusing on the connection between the vortex dynamics and scalar transport in the mixing enhancement process. In their simulation of control input, which mimics the flap actuator with the axisymmetric mode, they found the significance of streamwise vortical structures in the inner shear layer in the mixing enhancement

process. Through examination of the phase-averaged transport equation for the streamwise vorticity fluctuations, they found that streamwise vortices periodically appear with the control input.

In the present study, stereoscopic PIV is applied to the cross-stream plane of an actively controlled coaxial jet. This gives unique quantitative instantaneous information about the structure of the jet in its cross-section. The amplification of azimuthal instabilities and the subsequent evolution of the streamwise vortices are investigated. Mechanisms, by which the control input affects the streamwise vortices, are examined, and the impact of the streamwise vortices on the mixing enhancement between the inner and the outer jets is discussed.

2. Experimental setup

The coaxial jet facility consists of a central methane jet surrounded by an annular air jet issuing into the stagnant ambient air, see figure 1(a). The air in the outer jet passes through a honeycomb and five screens before entering the contraction with a contraction ratio of 25. The Reynolds number, based on the diameter of the outer jet, $D_0 = 20$ mm, and the outer jet bulk
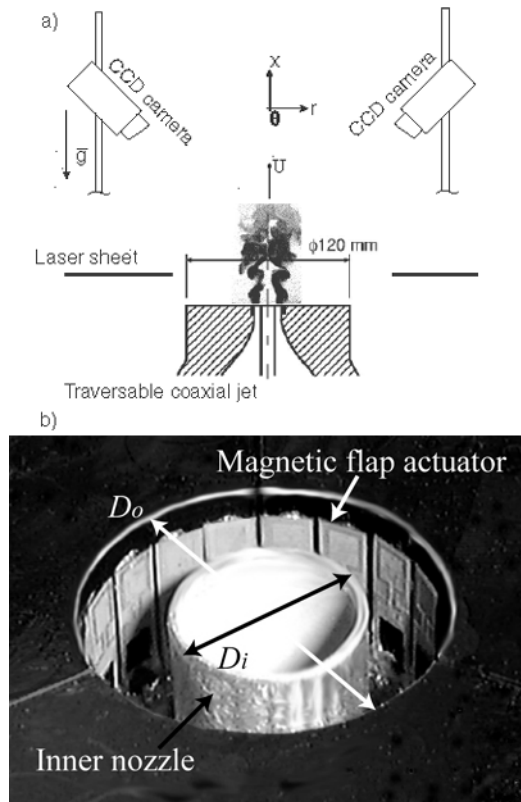

Figure 1. (a) The coaxial jet setup, the stereoscopic PIV arrangement for the cross-stream plane measurements and the cylindrical coordinate system. (b) Micro flap actuator nozzle.

velocity $U_{m,o} = 1.8$ ms^{-1}, is 2400. The central pipe has an outer diameter of $D_i = 10$ mm and the flow is fully developed laminar.

The outer to inner diameter ratio is 2, and the bulk velocity ratio is 5. The corresponding momentum flux ratio is 40.5. Under the present conditions, the flow field is dominated by the vortices in the outer shear layer of the outer jet [8]. Therefore, we placed the flap actuators on the inner surface of the outer jet.

The flow rates are carefully regulated by needle valves and mass flowmeters. The maximum velocity in the outer jet at the nozzle exit is $U_0 = 2.4$ ms^{-1}.

The wall thickness of the central pipe is 0.3 mm. Since the wall thickness is comparable to the momentum thickness of the inner boundary layer of the outer jet, its effect on the jet flow field cannot be neglected. However, as mentioned earlier, the jet dynamics is mainly governed by the vortices emerging at the outer shear layer, when the control input is applied. Therefore, the qualitative results in the present study should be free from the effect of the wall thickness.

2.1 *PIV setup*

The stereoscopic PIV arrangement for the cross-stream plane measurements in the cylindrical coordinate system is shown in figure 1(a). The jet setup itself is traversable both in the horizontal plane and in the streamwise direction. Thus, the same stereoscopic PIV calibration can be used for many measurements of different cross-stream planes. The angle between the CCD cameras was 90° in order to maximise the accuracy in the out-of-plane component [23]. The cameras (LaVision, FlowMaster 3S) contain 1024×1280 pixels and were equipped with Nikkor f105 lenses operating at f/11 ensuring a sufficient light intensity and particle image size for PIV purposes, as will be discussed in more detail later in this section. The field of view was chosen in order to enable the whole jet to be captured.

Willert et al. [29] showed that random errors due to poor light intensity became significant once the dynamic range in the light intensity was below 4 bits. The energy delivered by the 400 mJ double-pulsed Thales laser (532 nm), in combination with a distance of about 500 mm between the laser sheet and the cameras, ensured that the light intensity in the images was sufficient in this respect.

The camera frame rate and the laser repetition rate are 8 Hz. 500 image pairs were captured and subjected to averaging in all the cross-stream plane measurements. Note that the typical inverse time scale of the flow and the forcing ($St \approx 1.0$) corresponds to a frequency of 90 Hz with the present measurement conditions.

Solid SiO$_2$ particles ($\rho = 215$ kg m^{-3}) with a nominal diameter of 1.2 μm were employed as the tracer particles. These are introduced by letting the flow pass through glass vessels containing particles before entering the jet chamber. The relaxation time of the particles [20] is about 1 μs, which is much smaller than the Kolmogorov time scale, if estimated as $D_0^2 Re^{-3/2}/\nu = 227$ μs. Therefore, we can assume that the particles perfectly follow the flow. The number of particles inside each interrogation area (IA) is above the recommended value of 5 [12] to assure a good performance of the correlation technique.

The particle image diameter was above 2 pixels, and a Gaussian peak-fit was used for the sub-pixel interpolation in order to minimise peak-locking effects; see [28, 29]. Other PIV setup parameters were designed according to the criteria given by Angele and Muhammad-Klingmann [2] to minimise errors in the velocity statistics introduced by peak locking.

The images were captured and evaluated by commercial software (Davis, LaVision). The software also handles the calibration of the stereoscopic PIV. The images were evaluated with an adaptive multi-grid algorithm with a window offset, a normalised second-order correlation technique and a deformed IA in order to minimise errors introduced by velocity gradients.

The final size of IAs is 32×32 pixels, which corresponds to 0.68 mm $\times$ 0.68 mm. An overlap of 50% of the IA was used in all cross-correlations.

In order to remove spurious vectors, we employ the peak value ratio (PVR), which is defined as the ratio of the highest to the second highest peaks in the correlation plane. A criterion recommended by Keane and Adrian [12] is to set a limit at PVR = 1.2. This was used here together with range validation, discarding all velocities larger than the maximum inlet velocity. The valid detection rate (VDR) is varying between 90% and 99%. Outliers were replaced by interpolation, and subsequently a smoothing of the velocity field was applied prior to computing velocity gradients.

In the present stereoscopic PIV measurements in the cross-stream plane, the main flow is normal to the laser sheet. The laser sheet thickness was slightly broadened to 1.5 mm in order to allow for a larger timing to be used (150 μs) and to increase the effective seeding density. Two-dimensional (2D) PIV was also employed in the longitudinal plane in the same way as in [14]. Comparisons between the 2D PIV and the stereoscopic PIV measurements were made. The relative disagreement for the streamwise component was within 5% of U_0.

2.2 *Initial conditions*

An attempt was made to estimate the initial conditions of the coaxial jet using a small PIV measurement area. The velocity field was measured at the nozzle exit using an extension tube between the camera and the objective lens. This arrangement allowed for a measurement area of 2.9 mm $\times$ 2.3 mm. The spatial resolution with 32×32 pixels IAs becomes 73 μm. This is comparable to the typical spatial resolution for laser Doppler velocimetry (LDV). Two measurements were conducted in the radial direction covering the outer and part of the inner jet. The results are shown in figure 2. The mean velocity profile in the outer jet displays a weak top-hat shape due to the low Reynolds number flow condition. The disturbance level throughout the jet is of the order of 5%, which is slightly lower than that of the LDV measurements
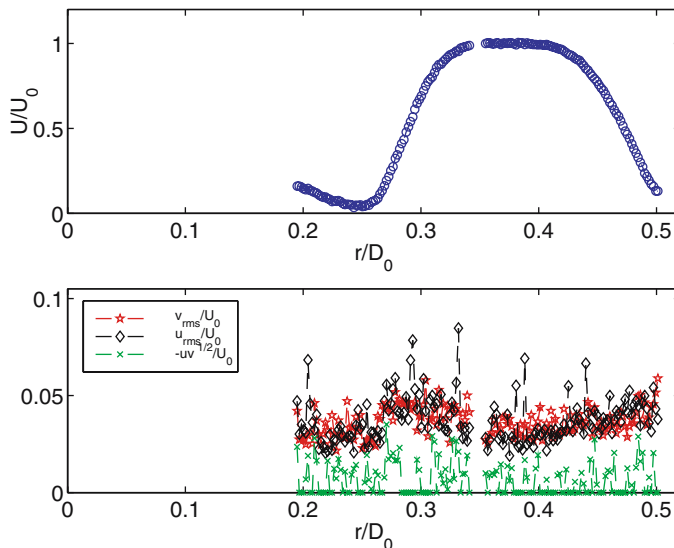

Figure 2. The mean velocity and the fluctuation level of the natural coaxial jet at the nozzle exit with the flaps present.

reported by Kurimoto et al. [14]. The momentum thickness of the outer shear layer of the outer jet is about 0.3 mm.

It was shown by Cohen and Wygnanski [6] that for a single natural jet, the axisymmetric mode is least stable if the ratio of the jet radius to the momentum thickness is larger than 6.5 at the end of the potential core, otherwise the helical mode is the least stable mode. The data by da Silva et al. [9] indicate that this criterion also holds for coaxial jets. According to this criterion the helical mode is the least stable mode in the present setup, since the momentum thickness is about $0.05D_0$ at $x/D_0 = 3$.

Note that the static flaps act as surface roughness. The evolution of streamwise vortices in the natural jet with a smooth nozzle without flaps is slightly slower than that in the nozzle with the flaps. However, the difference is much smaller than the dynamic effect of the control. Furthermore, the diameter of the streamwise vortices is unchanged with and without the flaps.

2.3 *Micro flap actuator nozzle*

The coaxial nozzle equipped with micro flap actuators, as shown in figure 1(b), was originally developed by Suzuki et al. [26]. The flaps are fabricated with micro electro-mechanical system (MEMS) technologies. The present prototype has 18 individually driven micro flap actuators positioned at the periphery of the outer jet nozzle exit, with an equal spacing in the circumferential direction. The flaps are 3 mm wide and cover 86% of the circumference. Unlike acoustic forcing, the flaps introduce a small localised disturbance in the outer shear layer. The present configuration allows one to vary not only the amplitude and frequency, but also the disturbance mode. The amplitude of the flap movement is kept constant in such a way that the flap-tip displacement becomes about 0.3 mm. The flaps are driven with a saw-wave signal. The frequency is varied in order to change the Strouhal number defined as $St = f D_0/U_{m,o}$. For a detailed description of the dynamics of the flap actuators, see [15, 26].

Employing the present nozzle, large-scale vortical structures are introduced in the outer shear layer and shed synchronised with the movement of the flaps. The different modes investigated here are the fundamental axisymmetric mode, the least-stable helical mode and the alternate mode. In the alternate mode, nine adjacent flaps are driven out-of-phase with the other nine [26]. The natural jet is also measured for reference.

2.4 *Vortex identification*

The quantity used here to detect a streamwise vortical structure is the second invariant of the deformation tensor:

$$Q = -\frac{\partial u_i}{\partial x_j}\frac{\partial u_j}{\partial x_i} \qquad (i, j = 2, 3), \qquad (1)$$

used, for example, by Adrian et al. [1]. In the present study, a local maximum in Q is taken as the centre of a vortex and the maximum value is taken as its strength. Only vortices with a strength higher than $0.5Q_{\text{threshold}}$ are considered, where $Q_{\text{threshold}}$ was taken as the average strength of the strongest primary vortex ring. The diameter of a vortex d was estimated based on the region around the vortex centre where Q was larger than $0.05Q_{\text{threshold}}$. Note that the diameter is an equivalent diameter of a circle with the same area as the detected region. The uncertainty of the vortex diameter determined in an instantaneous velocity field is about 1 interrogation area, which corresponds to about 10% when a vortex is $0.1D_0$ in diameter. However, the uncertainty of the mean vortex diameter drops to about 0.3% after the ensemble average over 1000 vortices.

3. Results: Primary vortices and jet evolution

3.1 *Primary vortical structures*

Figure 3 shows particle images in the longitudinal plane in the natural jet and the controlled jet for $St = 1.0$. Particles were introduced in the outer jet only. Figure 3(a) shows that the mixing between the inner and the outer jets is very poor in the near-field of the natural jet. The primary instability sets in around $x/D_0 \approx 1.25$ and leads to the formation of primary vortex rings. Figures 3(b)–(d) show that large-scale vortices are introduced by the control input. Vortical structures are formed both in the inner and the outer shear layers due to the large velocity ratio, as reported by Dahm et al. [8]. The inner vortex pinches off the inner jet, which promotes the mixing between the inner and the outer jets, whereas the outer vortex entrains ambient fluid. Figure 3(b) indicates that forcing with the axisymmetric mode leads to the formation of axisymmetric primary vortex rings. The alternate mode introduces two half primary vortex rings, which appear successively on either side of the jet, see figure 3(c). As noted by Kurimoto et al. [13], the vortices are slightly larger than those for the axisymmetric case and reach beyond the jet centre-line when pinching off the inner jet. Figure 3(d) shows the trace of the continuous helical vortex ring.

Figure 4 displays contours of phase-averaged Q in the longitudinal plane for the case of axisymmetric forcing for $St = 1.0$. The phase angle ϕ indicates the instant with respect to the movement of the flaps. As is evident, large-scale primary vortex rings shed synchronised with the movements of the flaps. The outer and inner vortices appear in a weakly staggered
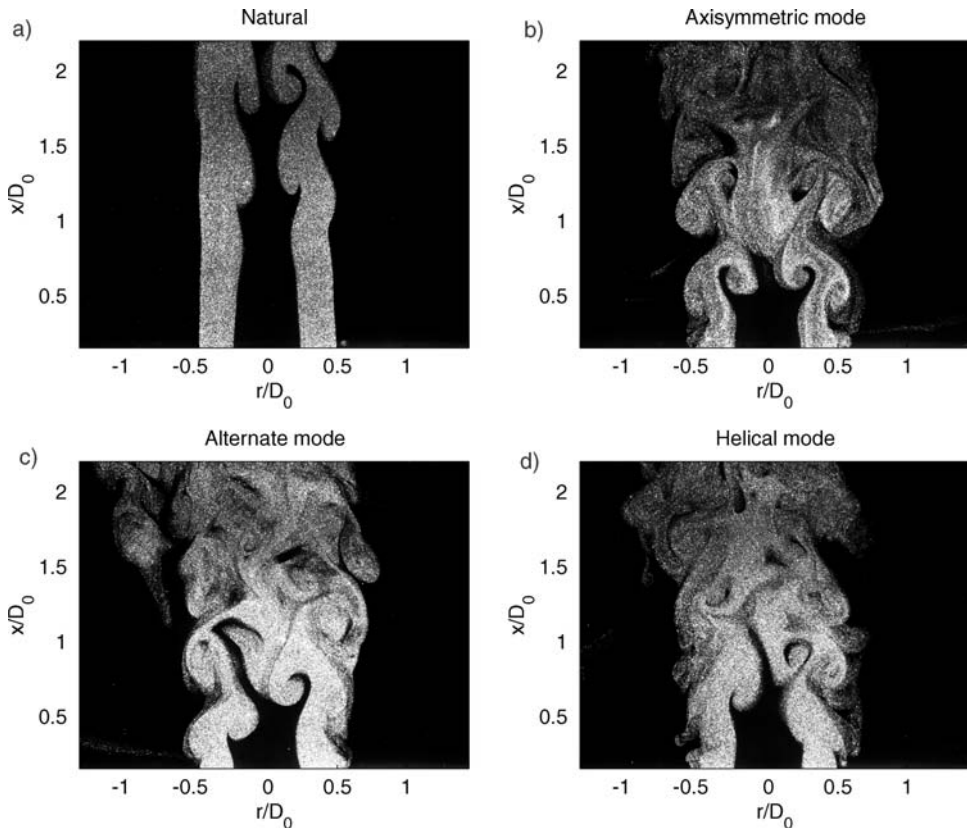

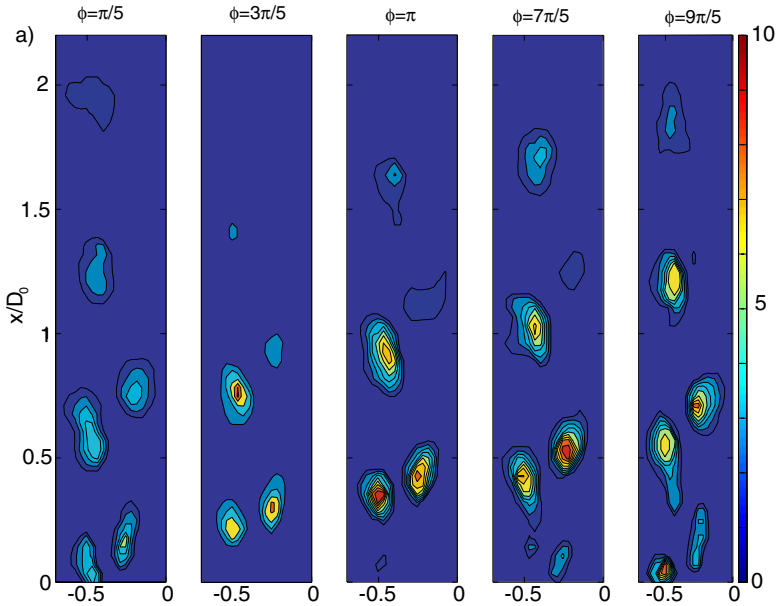Figure 3.   (a) Natural, (b) axisymmetric mode, (c) alternate mode, (d) helical mode at $St = 1.0$.

Figure 4.   Contours in the longitudinal plane of the phase-averaged normalised Q ($Q\mathbf{D}_0^2/\mathbf{U}_0^2$) for the axisymmetric forcing with $St = 1.0$.

counter-rotating pattern. The streamwise wavelength between the vortices originating from two subsequent flap cycles is approximately $0.5D_0$. The vortices are strong and coherent in the jet near-field before breakdown into turbulence at $xD_0 \approx 1.5$–2.0. The inner vortex ring breaks down earlier than the outer. The diameter of the jet and the magnitude of the streamwise velocity at a certain streamwise position are strong functions of the phase angle of the control, due to the passage of the primary vortices. This is most notable in the central jet around $x/D_0 = 0.75$. Differences with respect to the phase angle of the forcing become smaller further downstream. It is noted that with the non-axisymmetric forcing modes, primary vortices with a larger maximum value of Q appear in the near-field of the jet (not shown here).

3.2   *Jet evolution*

The streamwise mean velocity profiles from the cross-stream plane measurements (ensemble averaged and based on all azimuthal positions) are shown in figure 5. As can be seen, the evolution of the jet is more rapid for all the controlled cases compared to the natural jet, especially for the non-axisymmetric forcing mode. With the least-stable helical mode, the evolution is most accelerated. This indicates that the mixing between the inner and the outer jets is more enhanced for the helical mode than for the axisymmetric and the alternate modes. The difference between the control modes is most pronounced at $x/D_0 = 0.75$–1.0, where the intense mixing between the inner and the outer jets takes place [14]. Note that the effect of the control is larger in the inner jet, despite the fact that the control is applied to the outer shear layer.

4.   **Results: Streamwise vortices and secondary azimuthal instabilities**

We now turn our attention to the streamwise vortices and the instantaneous structure of the jet in the cross-stream plane. Figure 6(a) shows an instantaneous snap-shot in the cross-stream plane
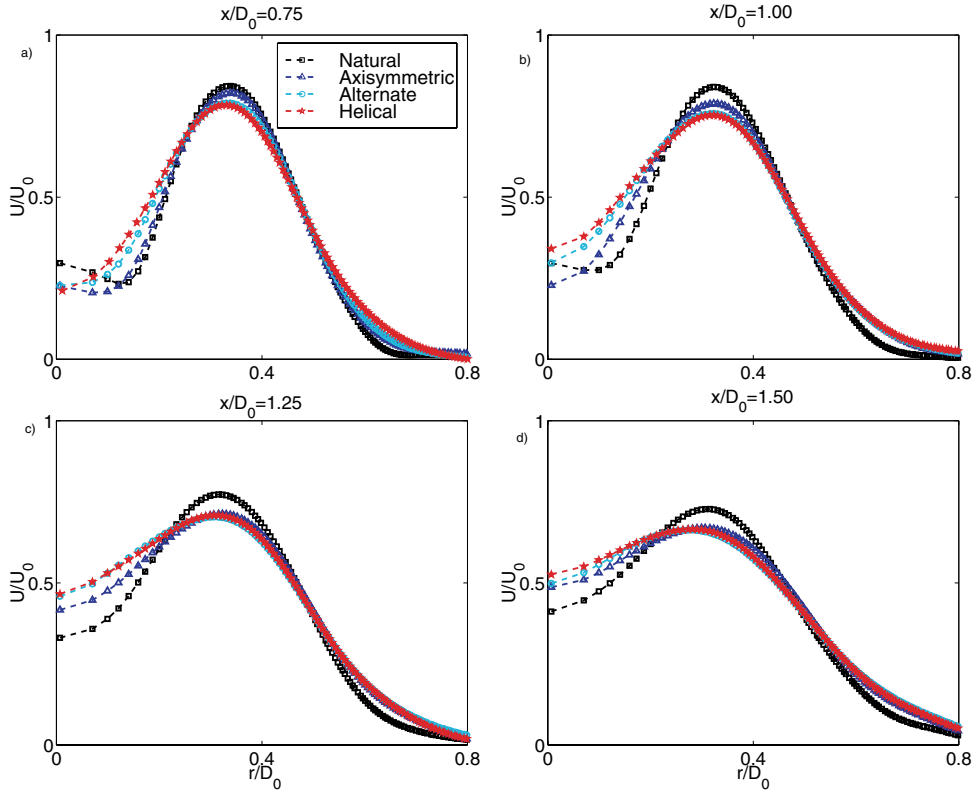
Figure 5. The effect of the different forcing modes on the streamwise mean velocity profile in the radial direction for $St = 1.0$.

of the jet at $x/D_0 = 1.0$ for the axisymmetric forcing mode with $St = 1.0$. The background contour corresponds to the magnitude of the normalised streamwise velocity U/U_0, and the velocity vectors indicate the instantaneous in-plane velocity components. Streamwise vortices are observed in the shear layer between the outer jet and the ambient fluid as well as that between the outer and the inner jets, where the azimuthal instability is present. Figure 6(b) shows an example of the instantaneous streamwise vortices, which are detected using the present algorithm. The region, which is detected as a streamwise vortex, is labelled with (⋆).

4.1 *Streamwise vortices*

Figure 7(a), (b) show the streamwise mean velocity profile in the radial direction together with the distribution of the count, strength and diameter of the streamwise vortices. The preferred position of the streamwise vortices is the radial position of the maximum shear, which coincides with the mean position of the primary vortex. This indicates that there is a connection between the streamwise and the primary vortical structures. The outer shear layer contains a larger count of streamwise vortices than the inner shear layer. As opposed to the simulation by Mitsuishi et al. [21], no specific differences were found for the streamwise vortices with respect to the phase angle of the control. This indicates that the streamwise vortices emerge randomly in the circumferential direction of the primary vortices, which are shed synchronised with the flap motion.
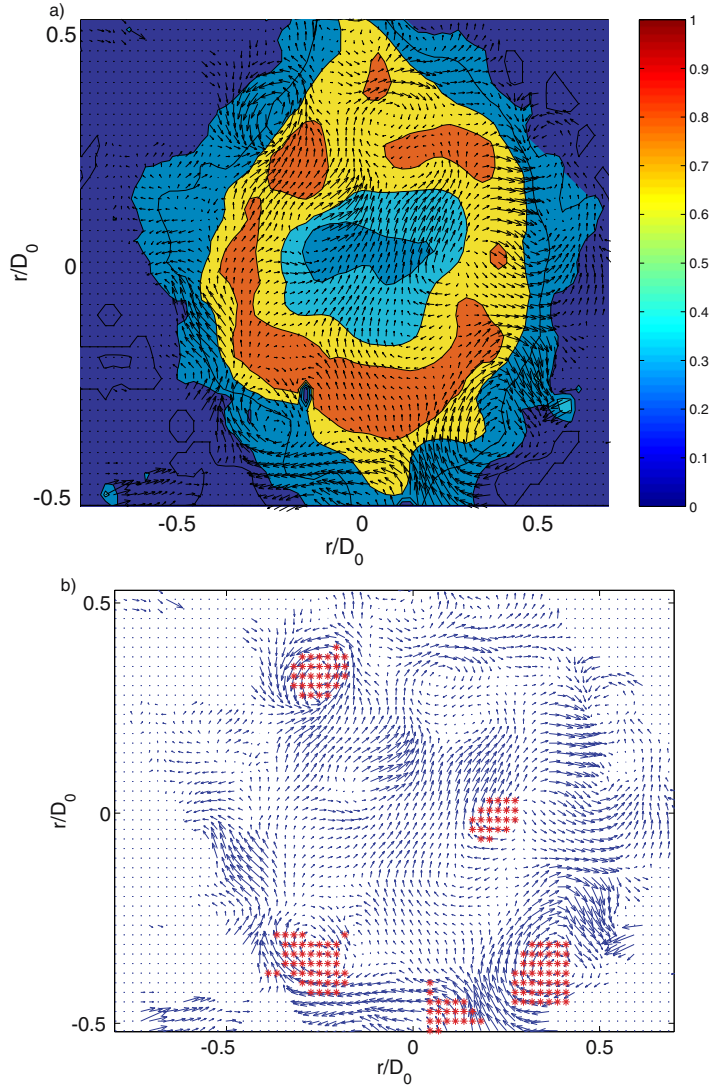
Figure 6.   (a) Normalised instantaneous streamwise velocity and in-plane velocity components in the cross-stream plane at $x/D_0 = 1.0$ for the axisymmetric forcing mode with $St = 1.0$. (b) Detected streamwise vortices using the present algorithm.

In figures 7(c), (d), each symbol corresponds to an instantaneous streamwise vortex in the inner ($+$) and the outer ($\circ$) shear layers. The results indicate that the strength and diameter of the vortices are related to the streamwise mean velocity gradient in the radial direction in a similar way as the count of the vortices.

Figure 8 shows $\langle Q \rangle$ versus d for the streamwise vortices in the outer shear layer $r/D_0 = 0.45$. It is found that stronger vortices are larger and smaller vortices are weaker, which is the opposite trend of what would be observed if the vortices were subjected to stretching.

All the trends of the streamwise vortices shown here hold irrespective of the phase angle, control mode and streamwise position.
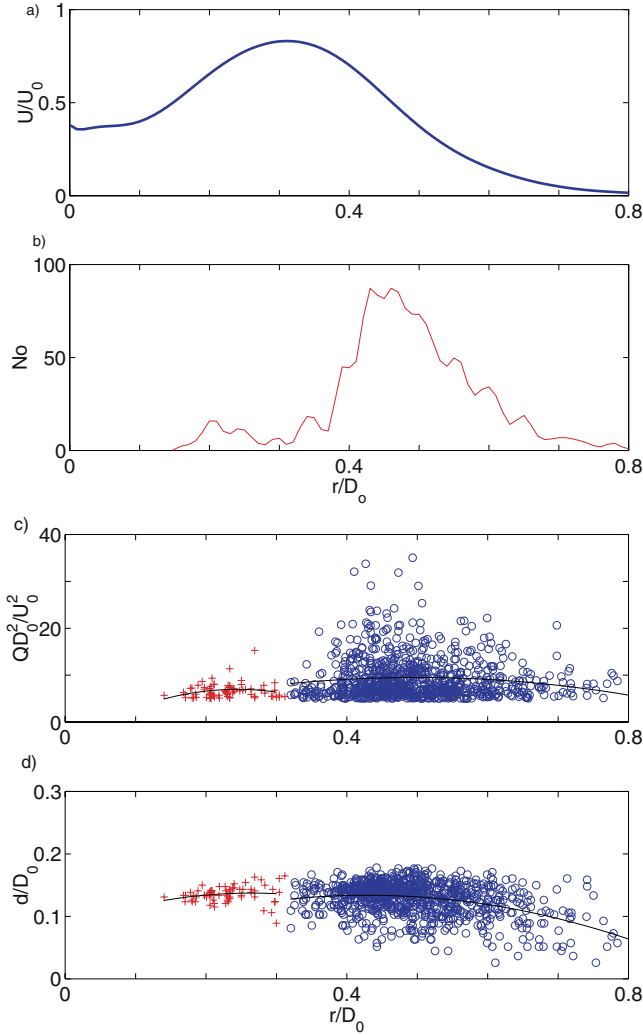
Figure 7. (a) Streamwise mean velocity profile in the radial direction. (b) Radial distribution of the counts of streamwise vortices. (c) The strength of the instantaneous streamwise vortices. (d) The diameter of the instantaneous streamwise vortices. The results are for one phase angle $\phi = 9\pi/5$ at $x/D_0 = 1.0$ for the axisymmetric forcing mode with $St = 1.0$.

4.1.1 The evolution of streamwise vortices in the downstream direction and the effect of control mode. The evolution of the streamwise vortices in the downstream direction is considered next. Figure 9 compares the ensemble-averaged quantities of the counts of vortices $\langle \text{No} \rangle$, the vortex diameter $\langle d \rangle / D_0$, and their strength $\langle Q \rangle D_0^2 / U_0^2$ for the inner and the outer shear layers and the different control modes. All the results are obtained for $St = 1.0$.

In the natural jet, streamwise vortices emerge in the outer shear layer at $x/D_0 \geq 1.25$, while they are practically absent in the inner shear layer for all streamwise positions. The counts of streamwise vortices increase in the downstream direction as reported by Lasheras et al. [16]. In all the controlled jets, the counts of the streamwise vortices are much larger than those in the natural jet. The evolution of the streamwise vortices is greatly enhanced by the control, and the development of the streamwise vortices becomes faster. As shown in figures 9(a), (d),
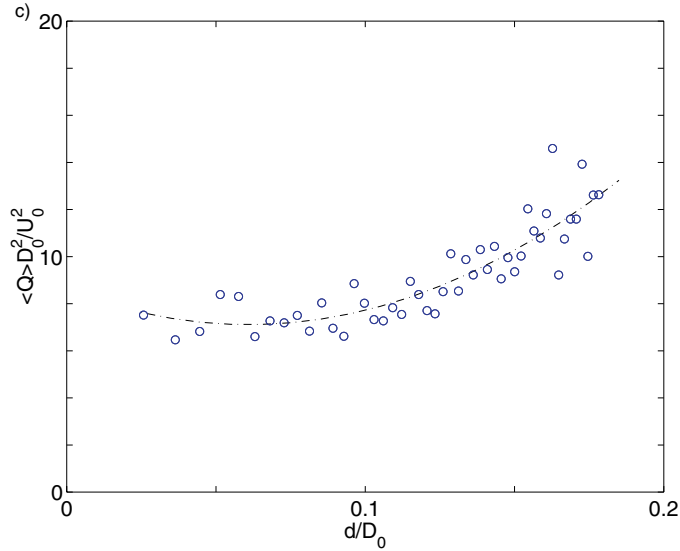
Figure 8.   The average strength as a function of the size of the streamwise vortices in the outer shear layer.

the least-stable helical mode provides the largest count in the jet near-field. This is in line with the earlier development of the streamwise mean velocity as shown in figure 5 and the increase in Q of the primary vortices (not shown here). At $x/D_0 \geq 1.25$, the count of the streamwise vortices approaches a similar level for all the control modes. The vortex count decreases downstream after they reach their maximum values at $x/D_0 \approx 1.5$. In the inner shear layer, the vortex count is almost three to four times smaller than that in the outer shear layer, although the trend is similar. It is noted that the vortex counts in both shear layers roughly reach their maximum capacity, which is estimated with the shear layer area and the vortex diameter as shown in figures 9(c), (f).

Figures 9(b), (e) show the evolution of the vortex strength. The vortex strength exhibits a trend similar to the vortex count, however less pronounced with respect to the control mode. The vortices in the inner shear layer are slightly weaker than the outer shear layer vortices. The streamwise vortices experience a maximum in their strength and counts further from the nozzle exit than the primary vortices. This implies that the relative importance of the streamwise vortices with respect to the primary vortices increases in the downstream direction, which is in accordance with the results of Liepmann and Gharib [17] for a single jet. Note that despite the local manipulation of the outer shear layer, the largest effect of the control in terms of the streamwise vortices is observed in the inner part of the jet.

The diameter of the streamwise vortices is relatively insensitive to the forcing mode as shown in figures 9(c), (f). It is noted that the vortex diameter in the outer shear layer continuously increases in the downstream direction and does not level off at $x/D_0 = 1.5$ (not shown here), indicating that it is governed by the thickness of the outer shear layer. (The growth rate of the vortex diameter is much smaller than the shear layer thickness though.) On the other hand, the vortex diameter in the inner shear layer is almost unchanged in the streamwise direction, whereas it is slightly larger than the diameter in the outer shear layer. This is an effect of the decrease in the extent of the inner shear layer.

Comparing to figure 4, one can conclude that the streamwise vortices are only slightly smaller and weaker than the primary vortices. This emphasise the significance of the streamwise vortices in the jet dynamics and their potential for mixing enhancement. Comparing the
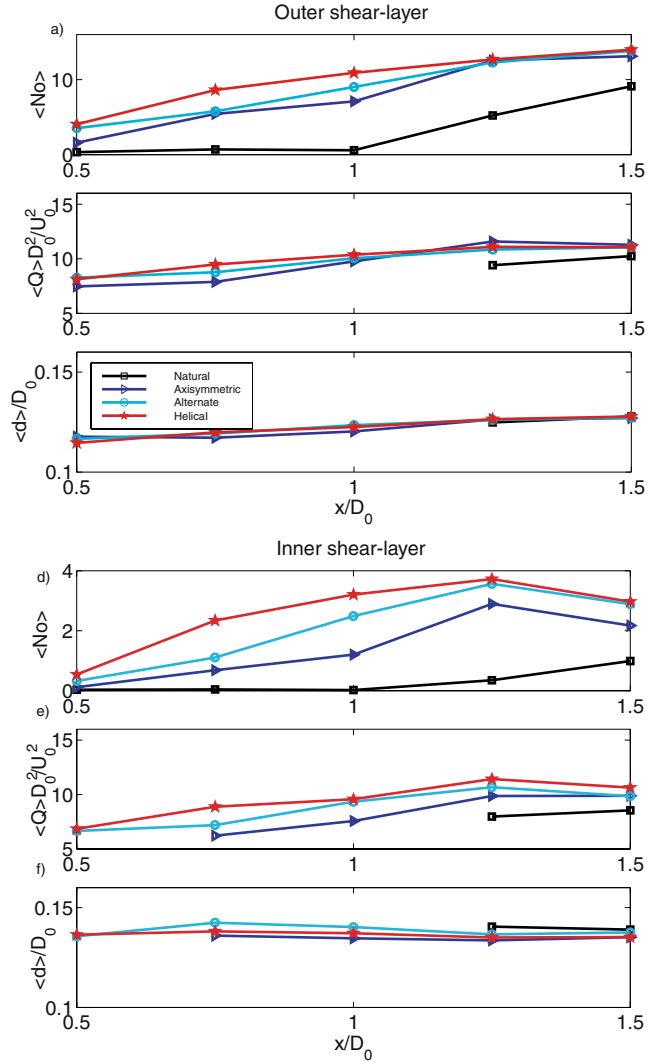
Figure 9. The evolution of the (a), (d) ensemble-averaged counts, (b), (e) strength and (c), (f) diameter of streamwise vortices for the different control modes for $St = 1.0$ and the natural jet with static flaps. Note that (a)–(c) corresponds to the outer shear layer and (d)–(e) to the inner shear layer.

present results of the streamwise vortices to the results from mixing measurements conducted in the same setup by Kurimoto et al. [14], one observes a strong connection between the onset of mixing between the inner and the outer jets, the presence of primary vortices and the appearance of streamwise vortices. This applies both to the natural and the axisymmetrically controlled jets. This shows the significance of the streamwise vortices for mixing in the present case, in line with the results of Breidenthal [4] for the plane mixing layer.

4.1.2 The effect of the Strouhal number of the forcing. Figure 10 shows the ensemble-averaged count, diameter and strength of the streamwise vortices for different St. It is clear that all the indices of the streamwise vortices have their peak values at $St \approx 1$–1.3, where the
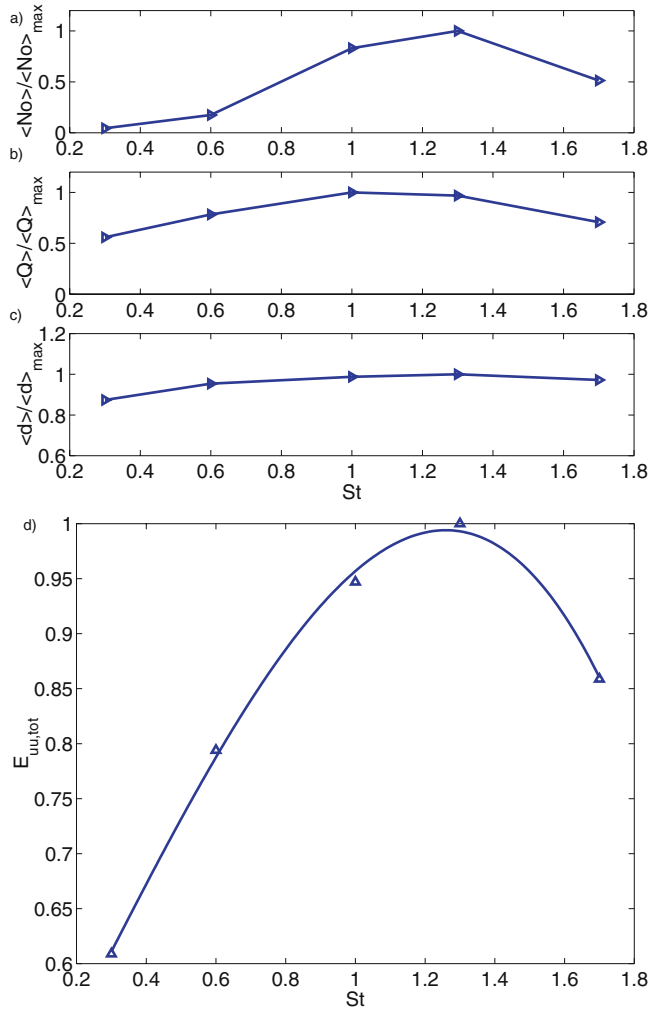
Figure 10.   The effect of *St* on the azimuthal instabilities and the streamwise vortices in the outer shear layer ($r/D_0 =$ 0.45) for the axisymmetric mode at $x/D_0 = 1$. (a) The average count, (b) strength and (c) size of the streamwise vortices, (d) the integrated azimuthal energy spectra. Note that all values are normalised with its maximum value.

magnitude of the primary vortices and the mixing between the inner and the outer jets are maximised [14].

4.2   *Azimuthal instabilities in the shear layers*

4.2.1   The evolution of the azimuthal instabilities in the downstream direction.   The mode number spectrum in the azimuthal direction was computed at the center-line of the inner and the outer shear layers where the magnitude of the velocity fluctuations is largest, and the primary and streamwise vortices are located.

Figure 10(d) shows the spectral energy normalised by U_0^2. The magnitude of the total energy in the azimuthal direction is maximised at $St \approx 1$. This indicates that there is a direct connection between the azimuthal instability of the primary vortices and the streamwise vortices.
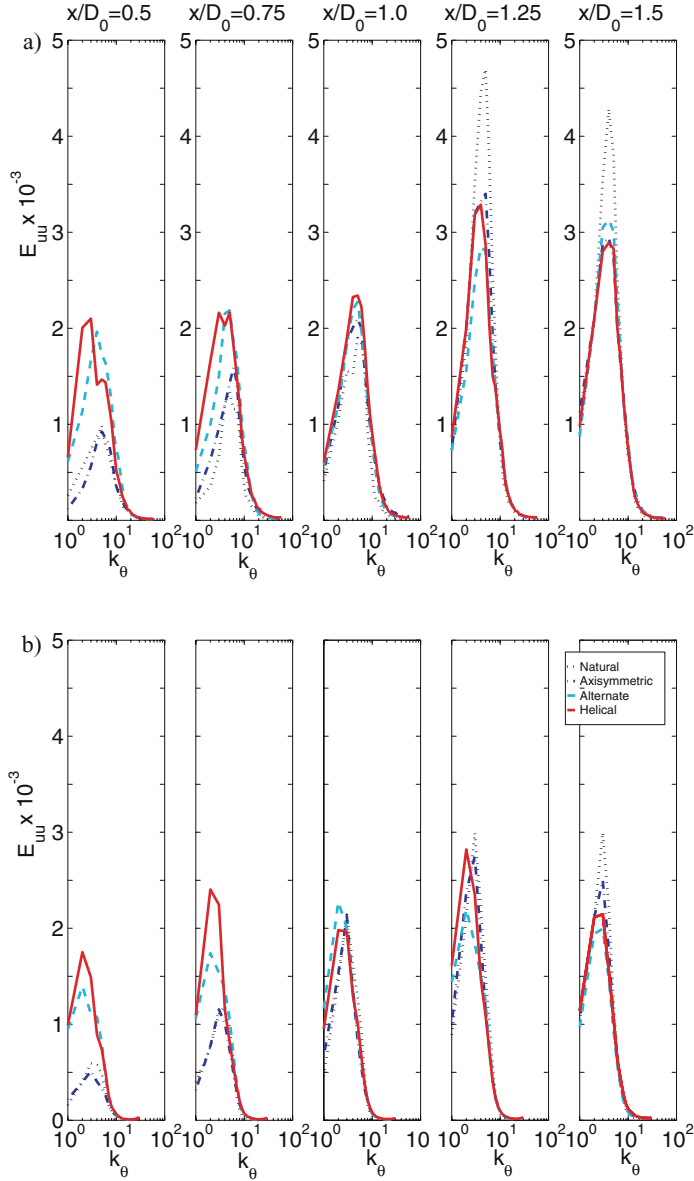
Figure 11. Azimuthal mode number spectra, $St = 1.0$ (a) outer shear layer ($r/D_0 = 0.45$), (b) inner shear layer ($r/D_0 = 0.25$).

Figure 11(a) shows the aziumthal mode number spectra for $St = 1$. The most energetic aziumthal mode number in the outer shear layer is around 4–5 for all the controlled jets. This is similar to that of the natural jet, which indicates that the optimal forcing, in this case the least-stable helical forcing, amplifies the natural instabilities of the jet. The azimuthal wavelength is found to be similar to the streamwise wavelength, which is in accordance with the observations in the plane shear layer [3, 22]. As shown in figure 11(b), the most energetic mode number in the inner shear layer is about half. Since the circumference is also half, the characteristic wavelength is the same. This is due to the fact that at the present high velocity

ratio, the vortical structures of the inner shear layer are governed by those of the outer shear layer [8]. Note that the wavelength remains unchanged in the downstream direction, in line with the results for a plane mixing layer [4].

The energy in the mode number spectra is increased in the streamwise direction for all the cases. For the controlled jets, the spectra are larger than in the natural jet and reach a maximum at $x/D_0 = 1.25$. This is most pronounced for the non-axisymmetric modes. The energy in the inner shear layer is overall lower than that in the outer shear layer.

4.2.2 Instantaneous azimuthal instabilities. Figure 12(a) shows typical instantaneous distributions of the streamwise velocity fluctuations in the azimuthal direction extracted from
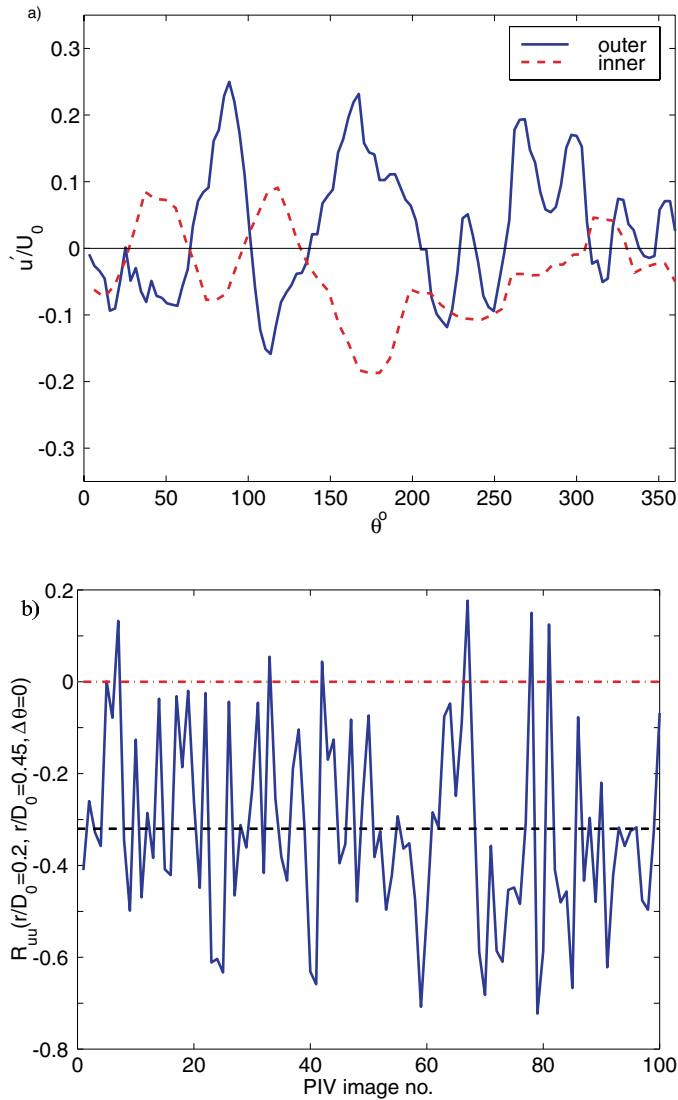

Figure 12.   (a) The instantaneous streamwise velocity fluctuations at $r/D_0 = 0.25$ and 0.45. (b) The instantaneous values of the correlation function between the inner and the outer shear layer for axisymmetric forcing, $x/D_0 = 1$ and $St = 1.0$.
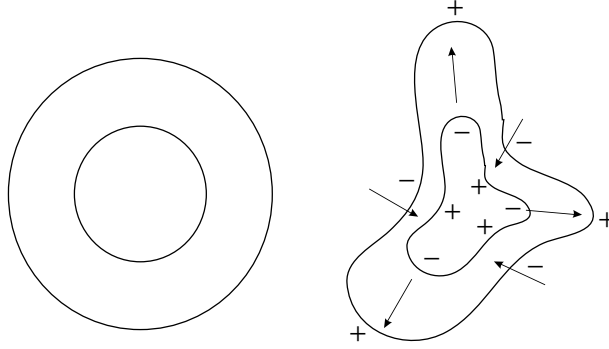
Figure 13. Simplified schematic picture of the instantaneous deformation of the jet which causes the fluctuations in the respective shear layers to be negatively correlated. The $+$ and $-$ signs indicate the effect on the fluctuations due to the deformation.

the centre-line of the inner and the outer shear layers at $x/D_0 = 1.0$. The control mode is the axisymmetric one with $St = 1.0$. Since the structure of the inner shear layer is governed by that of the outer shear layer, the velocity fluctuations in these shear layers are correlated, as can clearly be seen between $\theta = 20°$–$200°$. The negative correlation can be explained by the simple model as shown in figure 13. A part of the jet is deformed in the radial direction so that positive fluctuations in the outer shear layer are associated with negative fluctuations in the inner shear layer. Figure 12(b) shows the correlation function between the velocity fluctuations in the two shear layers, $R_{uu} = u'(r/D_0 = 0.20, \Delta\theta = 0)u'(r/D_0 = 0.45), \Delta\theta = 0)$. It is found that R_{uu} is negative for most of the instantaneous realizations. The average value of R_{uu} is about -0.3, which is indicated by the dashed line.

5. Conclusions

In the present study, a coaxial jet with a high velocity ratio was controlled by MEMS-fabricated micro flap actuators to allow for a flexible manipulation of shear layer vortices and mixing between the inner and the outer jets. Initially, the present control leads to the roll-up of primary vortices in the inner and the outer shear layers. Detailed information about the amplification of azimuthal instabilities and the subsequent evolution of streamwise vortices was obtained by applying stereoscopic PIV to the cross-stream plane of the jet. The following conclusions can be derived.

Streamwise vortices in the cross-stream plane are identified using the second invariant tensor of the deformation tensor, and their count, strength and diameter are examined. It is found that the streamwise vortices in general are only slightly smaller and weaker than the primary vortices, emphasising their significance in the jet dynamics and their potential for mixing. Their count and strength increase significantly in the downstream direction, whereas the strength of the primary vortices decreases. It is also found that the diameter and the strength of the streamwise vortices are positively correlated.

When the axisymmetric control mode is employed, the count and strength of the streamwise vortices become maximised for a flapping Strouhal number of unity, where the strength of the primary vortices are maximised. This is because the evolution of streamwise vortices is determined by the azimuthal instabilities of the primary vortices. Since Kurimoto et al. [14] report that the mixing is also maximised at $St \approx 1$, the streamwise vortices play a dominant role in the onset of mixing between the inner and the outer jets. It is also found that non-axisymmetric

forcing modes, in particular the least-stable helical mode, render an earlier development of the jet. This can be explained by an earlier development of the streamwise vortices.

Despite the fact that the present control utilises a local manipulation of the outer shear layer of the outer jet, the largest effect is observed in the inner part of the jet. The presence of streamwise vortices in the inner shear layer is a significant difference from the natural jet. It is conjectured that these vortices have a large contribution to the mixing enhancement.

The preferred azimuthal mode number is about 4–5 for all the control jets as well as for the natural jet, and independent of the streamwise position. It is also found that the characteristic wavelengths are the same in the inner and the outer shear layers. Since the fluid motion of the inner and the outer the shear layers is strongly coupled, the streamwise fluctuations in those shear layers are highly negatively correlated.

Acknowledgments

References

[1] Adrian, R.J., Meinhart, C.D. and Tomkins, C.D., 2000, Vortex organization in the outer region of the turbulent boundary layer. *Journal of Fluid Mechanics*, **422**, 1–54.
[2] Angele, K. and Muhammad-Klingmann, B., 2005, A simple model for the effect of peak-locking on the accuracy of boundary layer turbulence statistics in digital PIV. *Experiments in Fluids*, **38**(3), 341–347.
[3] Bernal, L. and Roshko, A., 1986, Streamwise vortex structure in plane mixing layers. *Journal of Fluid Mechanics*, **170**, 499–525.
[4] Breidenthal, R., 1981, Structure in turbulent mixing layers and wakes using a chemical reaction. *Journal of Fluid Mechanics*, **109**, 1–23.
[5] Chao, Y.-C., Jong, Y.-C. and Sheu, H.-W., 2000, Helical mode exitation of lifted flames using piezoelectric actuators. *Experiments of Fluids*, **28**, 11–20.
[6] Cohen, J. and Wygnanski, I., 1987 The evolution of instabilities in the axisymmetric jet. part 1. the linear growth of disturbances near the nozzle. *Journal of Fluid Mechanics*, **176**, 191–219.
[7] Corke, T.C. and Kusek, S.M., 1993, Resonance in axisymmetric jets with controlled helical-mode input. *Journal of Fluid Mechanics*, **249**, 307–336.
[8] Dahm, W.J.A., Frieler, C.E. and Tryggvason, G., 1992, Vortex structure and dynamics in the near field of a coaxial jet. *Journal of Fluid Mechanics*, **241**, 371–402.
[9] Demare, D. and Baillot, F., 2001, The role of secondary instabilities in the stabilization of a nonpremixed lifted jet flame. *Physics in Fluids*, **13**(9), 2662–2670.
[10] Ho, C.-M. and Huerre, P., 1984, Perturbed free shear layers. *Annual Review of Fluid Mechanics*, **16**, 205–234.
[11] Keane, R. and Adrian, R., 1992, Theory of cross-correlation in PIV. *Applied Scientific Research*, **49**, 191–215.
[12] Kurimoto, N., Suzuki, Y. and Kasagi, N., 2001, Active control of coaxial jet mixing and combustion with arrayed micro actuators. *Experimental Heat Transfer, Fluid Mechanics, and Thermodynamics*, pp. 511–516.
[13] Kurimoto, N., Suzuki, Y. and Kasagi, N., 2004, Active control of coaxial jet mixing with arrayed micro actuators. *Transactions of the Japanese Society of Mechanical Engineers*, 31–38.
[14] Kurimoto, N., Suzuki, Y. and Kasagi, N., 2005, Active control of lifted diffusion flames with arrayed micro actuators. *Experiments in Fluids*, **39**(6), 995–1008.
[15] Lasheras, J., Cho, J. and Maxworthy, T., 1986, On the origin and evolution of streamwise vortical structures in a plane, free shear layer. *Journal of Fluid Mechanics*, **172**, 231–258.
[16] Liepmann, D. and Gharib, M., 1992, The role of streamwise vorticity in the near-field entrainment of round jets. *Journal of Fluid Mechanics*, **245**, 643–668.
[17] Martin, J. E. and Meiburg, E., 1991, Numerical investigation of three-dimensionally evolving jets subject to axisymmetric and azimuthal perturbations. *Journal of Fluid Mechanics*, **230**, 271–318.
[18] Martin, J. E. and Meiburg, E., 1992, Numerical investigation of three-dimensionally evolving jets under helical perturbations. *Journal of Fluid Mechanics*, **243**, 457–487.
[19] Melling, A., 1997, Tracer particles and seeding for particle image velocimetry. *Measurement Science and Technology*, **8**, 1406–1416.
[20] Mitsuishi, A., Fukagata, K. and Kasagi, N., 2005, On the relationship between large-scale vortical structures and scalar transport processes in a controlled confined coaxial jet. *Proc. 4th Turbulence and Shear flow phenomena, Williamsburg*, 841–846.

[21] Pierrehumbert, R. and Widnall, S., 1981, The structure of organized vortices in a free shear layer. *Journal of Fluid Mechanics*, **102**, 301–313.
[22] Prasad, A.K., 2000, Stereoscopic particle image velocimetry. *Experiments in Fluids*, **29**, 103–116.
[23] Reeder, M.F. and Samimy, M., 1996, The evolution of a jet with vortex generating tabs: real time visualization and quantitative measurements. *Journal of Fluid Mechanics*, **311**, 73–118.
[24] Rehab, H., Villermaux, E. and Hopfinger, E.J., 1997, Flow regimes of large-velocity-ratio coaxial jets. *Journal of Fluid Mechanics*, **345**, 357–381.
[25] da Silva, C.B., Balarac, G. and Métais, E., 2003, Transition in high velocity ratio coaxial jets ananlysed form direct numerical simulation. *Journal of Turbulence*, **4**, 0–24.
[26] Suzuki, H., Kasagi, N. and Suzuki, Y., 2004, Active control of an axisymmetric jet with distributed electro-magnetic flap actuators. *Experiments in Fluids*, **36**, 498–509.
[27] Villermaux, E. and Rehab, H., 2000, Mixing in coaxial jets. *Journal of Fluid Mechanics*, **425**, 161–185.
[28] Westerweel, J., 1997, Fundamentals of digital particle image velocimetry. *Measurement Science & Technology*, **8**, 1379–1392.
[29] Willert, C., Raffel, M., Kompenhans, J., Stasicki, B. and Kähler, C., 1996, Recent applications of Particle Image Velocimetry in aerodynamic research. *Flow Measurement and Instrumentation*, **7**(3/4), 247–256.